CMS PAS SUS-09-002

DRAFT
CMS Physics Analysis Summary

2009/05/19
Archive Id: 1.8
Archive Date: 2009/05/19 08:15:22
Archive Tag: PAS

Discovery potential and measurement of a dilepton mass edge in SUSY events at $\sqrt{s} = 10$ TeV

The CMS Collaboration

Abstract

Within the minimal supergravity model (mSUGRA), the observability of the decay of the next to lightest neutralino into leptons has been studied using the full simulation of the CMS detector. The final state signature consists of two opposite sign leptons, several hard jets and missing transverse energy. Using three different minimal supergravity benchmark points the possible discovery of a mSUGRA signal is studied. The expected precision of the measurement of the dileptonic mass edge is reported for 200 pb^{-1} and 1 fb^{-1} of data, including systematic and statistic uncertainties and comparing different decay signatures.

1 Introduction

The standard model of particle physics (SM) leads to a number of unsolved issues like the hierarchy problem and it provides no solution for pressing questions arising from astrophysical observations, most notably dark matter. In Supersymmetry (SUSY) a natural candidate for dark matter can be found if R-parity conservation is assumed. Supersymmetric particles (sparticles) have not been observed up to now which implies that they have to be heavy. On the other hand to provide a solution to the hierarchy problem their masses have to be in the TeV range.

The long anticipated start of the Large Hadron Collider (LHC) in 2009 will allow to explore this new TeV range. With its center of mass energy of 10 TeV in 2010 it will allow to probe supersymmetric models very early on. A key point after discovery will be the determination of the sparticle properties. If R-parity is conserved the lightest neutralino escapes detection and no mass peaks can be observed in SUSY decay chains. Of special interest are robust signatures such as mass edges in leptonic final states which can be probed with the CMS experiment.

The purpose of this analysis is to observe a significant excess of opposite sign same flavour leptons over the various backgrounds and to measure the endpoint in the invariant mass distribution. All flavour symmetric background (including SUSY decays of this type) can be determined from data events with opposite sign opposite flavour leptons. The aim is to perform such an analysis already with the first LHC data which is expected to amount to roughly 200-300 pb^{-1} in 2010.

2 Signal

Three minimal supergravity benchmark points (Tab.1) have been studied to cover different decay modes of the neutralinos within supersymmetry. The mass spectra of the three benchmark points have been calculated using the SOFTSUSY code [1]. All branching ratios have been calculated with the SUSYHIT program [2] and the events are simulated using PYTHIA [3]. The k-factor for the cross section at 10 TeV is calculated using a modified version of PROSPINO 2 [4]. In mSUGRA there are very long decay chains leading to several hard jets. The escaping neutralino leads to missing transverse energy. This facts allow to define a search region to observe an excess over the SM and are used as main event selection criteria as described in Sec. 4.

Table 1: mSUGRA benchmark points LM0, LM1 and LM9.

	m_0 [GeV]	$m_{1/2}$ [GeV]	A_0 [GeV]	$\tan\beta$	sign μ	σ_{LO} [pb]	σ_{NLO} [pb]	$m_{ll,max}$ [GeV]
LM0	200	160	-400	10	+1	110.0	151.8	52,7
LM1	60	250	0	10	+1	16.1	21.7	78,2
LM9	1450	175	0	50	+1	11.1	18.2	62,9

Additionally the leptonic decay of the next to lightest neutralino leaves a characteristic signature. This decay can proceed in different ways even in the mSUGRA model. A mass difference of the neutralinos smaller than the Z boson mass and any slepton mass leads to a three body decay. In that case the endpoint in the lepton invariant mass represents directly the mass difference of the two lightest neutralinos

$$m_{ll,max} = m_{\tilde{\chi}_2^0} - m_{\tilde{\chi}_1^0}. \quad (1)$$

The shape of the distribution depends on the mSUGRA parameters.

A two body decay occurs via a real slepton and is allowed if at least one slepton is lighter than the mass difference of the neutralinos. In that case the endpoint can be expressed by

$$(m_{ll}^{max})^2 = \frac{\left(m_{\tilde{l}}^2 - m_{\tilde{\chi}_2^0}^2\right)\left(m_{\tilde{\chi}_2^0}^2 - m_{\tilde{\chi}_2^0}^2\right)}{m_{\tilde{l}}^2}, \tag{2}$$

where $m_{\tilde{l}}$ is the mass of the intermediate slepton. The shape of the mass edge results only from kinematics and is triangular. At LM0 the 3-body decay mode is present as for LM9, while at LM1 the 2-body decay is possible shown in App. A for the three LM benchmark points at parton level.

If the mass difference matches the Z boson mass this leads to an enhanced Z boson production accompanied by large missing transverse energy and several hard jets. This signature is not in the focus of the present analysis. It has been studied for example in [5]. Another possibility in mSUGRA is a decay predominantly through the lightest Higgs boson which leads to a different signature as well.

3 Physics objects

The datasets with a vector boson or a $t\bar{t}$-pair have been simulated using the MADGRAPH matrix element generator [6]. The parton shower and hadronisation is modelled in PYTHIA. The di-jet, quarkonia, Wγ and Zγ samples are simulated using PYTHIA. All samples undergo the full CMS detector simulation.

The samples have been scaled to next to leading order cross sections. For the SUSY samples the k-factor calculated with PROSPINO 2 has been used. The k-factor for the $t\bar{t}$ sample of 1.3 has been derived from [7]. The k-factors of the Z+jets and the W+jets samples of 1.14 have been derived from [8]. For the di-jet sample no k-factors are applied.

The datasets where produced during the Summer 08 Monte Carlo (MC) production. The MC production was targeted of an integrated luminosity of 200 pb^{-1} and used ideal calibration and alignment constants.

Each muon has to be identified as a global muon, which includes a reconstruction in both the muon system and the inner tracker [9]. The track of the muon in the inner tracker has to have at least 11 hits and a χ^2/ndf below 10. Additionally a $p_T > 10$ GeV and $|\eta| < 2$ is required for each muon. The impact parameter of the muon track which is corrected for the beam-spot position is required to be below 2 mm and this cut could be tightened if necessary (the current set of events does not include misalignment so a too tight cut could overestimate the efficiency in real data).

Each electron has to fulfill the tight electron identification criteria, which consist of a set of cuts depending on the electron p_T and η [10]. Additionally a $p_T > 10$ GeV and $|\eta| < 2$ is required for each electron. The impact parameter of the electron track which is corrected for the beam-spot position is required to be below 2 mm as in the muon case.

A combined relative lepton isolation has been used. The isolation uses information from both calorimeters and the silicon tracker. The isolation value (Iso) is given by the ratio of the sum of all (subtracting the lepton) E_T or p_T objects within a cone in η-ϕ-space of $\Delta R = \sqrt{\Delta\eta^2 + \Delta\phi^2} <$

0.3 around the lepton and the lepton p_T. It has been calculated using

$$Iso = \frac{\sum\limits_{ECAL} E_T + \sum\limits_{HCAL} E_T + \sum\limits_{tracks} p_T}{p_T} \tag{3}$$

where the first sum runs over transverse energy in the electromagnetic calorimeter, the second sum runs over the transverse energy in the hadronic calorimeter and the third sum runs over the transverse momentum deposited in the tracker within the cone subtracting the lepton.

The isolation for muons and electrons is shown in App. B. The cut value is chosen to be $Iso <$ 0.2 for muons and the cut is placed at $Iso < 0.4$ for electrons, to obtain a similar rejection and efficiency for electrons and muons.

The jet algorithm is a seedless infrared safe cone algorithm (SIScone) [11] with a cone size of 0.5 in ΔR. The jets are corrected using MC jet energy corrections [12]. Each corrected jet is required to have a $p_T > 30$ GeV and the jet axis has to be within $|\eta| < 2.5$. Additionally the overlap of the jets with the electrons is checked and a jet is vetoed if an electron shares its supercluster with the jet. The missing transverse energy (MET) is based on the calorimeter information and is corrected for muon energy deposition and jet energy scale [13].

3.1 Efficiency measurement

Since the muon and electron reconstruction efficiencies are not equal these efficiencies have to be measured from data. Therefore a "tag and probe" method using events with a Z boson is used. To select clean Z events a tight selection is applied to one lepton (tag) and only loose criteria are used on the probe side. Similar studies are presented in [14]. For this analysis a Z sample including all backgrounds with an integrated luminosity of 100 pb^{-1} has been used.

The tag has to fullfil the lepton selection criteria described in Sec. 3. Additionally a $p_T > 20$ GeV is required and the tag has to be reconstructed within $|\eta| < 1$. As probes all tracks in the event which have a $p_T > 10$ GeV within $|\eta| < 2$ are used. The invariant mass of the tag and the probe is required to be in the range of the Z boson mass ($80GeV < m_{tag,probe} < 100$ GeV). The efficiency is calculated simply by counting the number of events where the probe can be matched to a reconstructed lepton with a $p_T > 10$ GeV (within $\Delta R < 0.1$), which passes the lepton selection criteria described in Sec. 3.

The distribution of all tag and probe pairs for muons and electrons is shown in App. C. As expected the pairings do not consist purely of Z events and include also backgrounds mainly from di-jet and W events. These events would distort the efficiency measurement and therefore this background is measured from data by selection of same sign tag and probe pairs. The number of background events is simply two times the number of same sign pairs since in background events the number of same sign pairs should be the same as the number of opposite sign pairs $N_B = 2 \cdot N_{SS}$. We are aware of the potential bias due to a charge correlation of the tag and probe pair in W boson events and we do not account for a possible charge misreconstruction efficiency because it should give only a small correction to the obtained results [14]. We include a potential bias of $\pm 5\%$ in the efficiency calculation in the study of the systematic uncertainties.

The efficiency can simply be calculated using

$$\epsilon = \frac{N_{pass} - N_{B,pass}}{N_{probe} - N_{B,probe}}, \tag{4}$$

where N_{pass} is the number of probes that can be matched onto a reconstructed lepton, N_{probe} the number of probes and N_B the number of background events from the same sign selection.

The efficiency is calculated in bins of η and p_T. Since the statistic is largest in the bulk region of the Z sample (lepton p_T around 50 GeV) the binning is chosen accordingly. The efficiency versus p_T for muons and electrons is shown in App.C. A good agreement between the tag and probe results and MC expectation is found.

Table 2: Global efficiencies obtained with the tag and probe method compared to MC truth.

	N_{pass}	$N_{B,pass}$	N_{probe}	$N_{B,probe}$	ϵ_{TnP}	ϵ_{MC}
Muons	60028 ± 245	4 ± 2	68679 ± 262	6662 ± 81	0.968 ± 0.013	0.964 ± 0.003
Electrons	34550 ± 185	690 ± 26	50164 ± 223	12400 ± 111	0.897 ± 0.010	0.881 ± 0.003

These efficiencies have been used to correct the invariant mass distributions of the lepton pairs. Each lepton in the distributions is weighted by $1/\epsilon$. The tag and probe method could be refined if necessary at a higher luminosity but for this analysis the expected precision is sufficient (Tab. 2 shows the global results from both methods).

4 Event selection

The base selection requires two leptons of opposite sign. We do not require two same flavour leptons in order to measure the background events directly from the same dataset as described in Sec. 4.1. The main SUSY selection is based on jets and missing transverse energy. The cuts have not been optimised at a certain benchmark point, but should reflect the general SUSY signature. The selection requires three jets with $p_T^{j1} > 100$ GeV, $p_T^{j2} > 50$ GeV, and $p_T^{j3} > 50$ GeV. Additionally a missing transverse energy of at least 100 GeV is required.

In this analysis we require two single leptonic high level trigger (HLT) paths to select the events. Since the leptons originating from the signal decay have a very soft p_T spectrum we use the triggers with the lowest available threshold for electrons (15 GeV) and muons (11 GeV).

Due to the SUSY signature of hard jets and missing transverse energy there exists the possibility to use a single hadronic trigger path to recover possible inefficiencies of the leptonic triggers and we compare their efficiencies to hadronic trigger path efficiencies.

We observe an efficiency (in the inclusive SUSY sample) of $96.1 \pm 0.5\%$ for the isolated leptonic paths with respect to the final event selection. The most efficient hadronic trigger path yields an efficiency of $97.9 \pm 0.4\%$ using the single jet trigger with a threshold of 110 GeV.

The number of events obtained after each cut is listed in Tab. 3. After HLT selection the sample is still dominated by di-jet and W events. The requirement of two isolated and well identified opposite sign leptons rejects most of the di-jet events and the selection is dominated by events with a Z boson. After requirement of three hard jets a SUSY inclusive signal to background ratio of roughly one can be reached. After requirement of missing transverse energy the main background from the standard model consists of $t\bar{t}$-events. With the described selection an efficiency of 25% on the signal events is obtained. At the studied benchmark point LM0 a high number of SUSY background events is found (flavour symmetric background from chargino decays) which is irreducible. This complicates the discovery of this decay at this point as described in Sec. 5.3.

Table 3: Number of selected events using the described event selection for an integrated luminosity of 200 pb^{-1}.

	σ_{LO} [pb]	k-factor	HLT	$\geq$ 2 leptons	$\geq$ 3 jets	MET
LM0 signal	1.0	1.38	362	226	128	86
LM0 inclusive	110.0	1.38	8067	1021	546	366
tt+jets	319.0	1.3	25655	2474	245	84
Z+jets	3700.0	1.14	541013	190032	409	1
W+jets	40000.0	1.14	3108397	358	5	2
Diboson	51.9	1.0	5444	911	2	0
Di-jets	2003572.9	1.0	2801134	1116	4	0

4.1 Statistical measurement of the background events

All background which leads to uncorrelated lepton pairs can be measured directly from data [15]. Therefore we select the opposite sign opposite flavour lepton pairs and use this distribution to extrapolate to the same flavour opposite sign lepton pair distribution.

With this method one is able to predict all backgrounds which produce uncorrelated leptons such as W, $t\bar{t}$, di-jet and WW events.

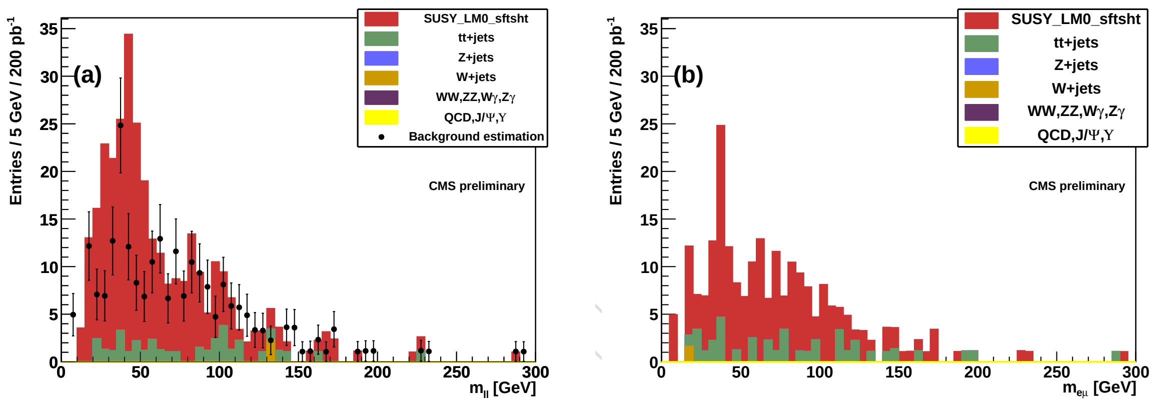

Figure 1: The same flavour opposite sign lepton pair distribution including all cuts is shown in (a). Black points represent the extrapolation from (b), which displays the opposite flavour opposite sign lepton pairs. No scaling has been applied but exactly 200 pb^{-1} of MC events have been analysed.

The invariant mass distribution of all opposite sign same flavour leptons for 200 pb^{-1} is shown in Fig. 1(a). In this plot no scaling has been applied but only the number of expected events in 200 pb^{-1} has been analysed. The opposite sign opposite flavour distribution used to extrapolate the background is displayed in Fig. 1(b). One can see that at a low luminosity the statistical fluctuations are relatively large. Therefore the background is modelled and fitted as described in Sec. 5.

5 Determination of the mass edge

The model used for the fit of the mass edge consists of three parts. To model the signal a quadratic term convoluted with a gaussian has been used in case of a 3-body decay

$$S(m_{ll}) = \frac{1}{\sqrt{2\pi}\sigma} \int_{0}^{m_{cut}} dy \cdot y^2 e^{\frac{-(m_{ll}-y)^2}{2\sigma^2}}. \tag{5}$$

In case of the two-body decay the signal model consists of a triangle convoluted with a gaussian

$$T(m_{ll}) = \frac{1}{\sqrt{2\pi}\sigma} \int_{0}^{m_{cut}} dy \cdot y e^{\frac{-(m_{ll}-y)^2}{2\sigma^2}}. \tag{6}$$

The decision which function is fitted to the background is based on a "goodness of fit" (χ^2) test of each fit. A curve parametrized as

$$B(m_{ll}) = m_{ll}^{a} \cdot e^{-b \cdot m_{ll}} \tag{7}$$

has been used to fit the opposite sign opposite flavour invariant mass distribution. Additionally the Z peak is fitted using a Breit-Wigner convoluted with a gaussian.

The fits are performed within the RooFit package [16] based on an unbinned and extended maximum likelihood fit to the di-lepton invariant mass distribution

$$L = \frac{e^{-\left(N_{Sig}+N_{Bkg}+N_Z\right)}}{\left(N_{Sig}+N_{Bkg}+N_Z\right)!} \prod_i \left[N_{Sig} P_S \left(m_{ll}\right)_i + N_{Bkg} P_B \left(m_{ll}\right)_i + N_Z P_Z \left(m_{ll}\right)_i\right]. \tag{8}$$

Here $P_S = S$ or $P_S = T$ is the signal probability density function (triangle or quadratic term convolved with a gaussian), P_B is the background model and P_Z is the Breit-Wigner function convoluted with a gaussian. The number of signal N_{Sig}, background N_{Bkg} and Z events N_Z are fitted as well.

5.1 Resolution measurement

The resolution smearing of the detector, which is used in the fit function (Eq. 5+6), is measured from Z events. The selection using two well identified opposite sign leptons is used without any additional event selection cuts. In the two distributions for electrons and muons a Bifurcated Gaussian (with different widths on each side of the mean)

$$G_{BF}\left(m_{ll}\right) = \begin{cases} \frac{1}{\sqrt{2\pi}\sigma_L} e^{\frac{-(m_{ll}-m)^2}{2\sigma_L^2}}. & m_{ll} \leq m \\ \frac{1}{\sqrt{2\pi}\sigma_R} e^{\frac{-(m_{ll}-m)^2}{2\sigma_R^2}} & m_{ll} > m \end{cases} \tag{9}$$

is fitted to account for the asymmetry in the distribution. The detector resolution is averaged from the two resolution values obtained from the fit subtracting the natural Z boson width. The values of the resolution parameter in the convolution is used in the final fit in Sec. 5.2. The fit of the resolution is shown in App. D and the values obtained are shown in Tab. 4.

Table 4: Resolution measurement from Z events.

	$\sigma_{\mu\mu}$	σ_{ee}	σ_{ll}
Resolution [GeV]	1.33 ± 0.07	1.96 ± 0.09	1.61 ± 0.06

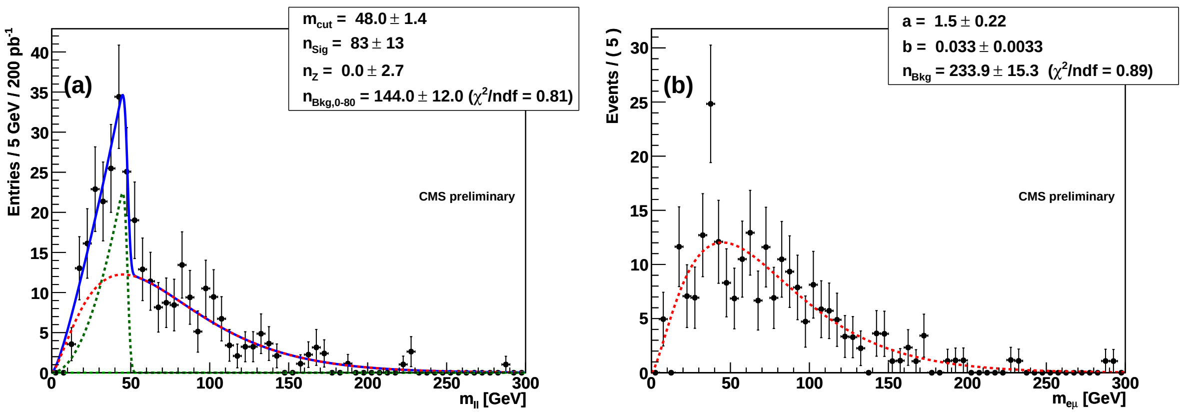

Figure 2: The combined fit at LM0 for 200 pb^{-1} is shown in (a). The green curve represents the SUSY signal model, the red curve is the background function and the light green dashed line the Z contribution. The black points represent the MC events. In (b) the fit of the background function to the $e\mu$ invariant mass distribution is shown.

5.2 Fit of the mass edge for 200 pb^{-1} at LM0

Using all information derived up to this point one can perform a fit to the invariant mass distribution of opposite sign lepton pairs. For this fit a dataset of exactly 200 pb^{-1} has been analysed to perform one pseudo experiment.

The fit to the invariant mass distribution at LM0 is shown in Fig. 2(a). It yields a value of

$$m_{ll,max} = (48.0 \pm 1.4)\ \text{GeV}. \tag{10}$$

The derived number of signal events $n_{sig} = 83 \pm 13$ agrees with the number of signal events from MC truth (Tab. 3). The theoretical endpoint $m_{ll,theo} = 52.7$ GeV is 4 GeV away from the fitted value. This is taken into account in the systematic uncertainty which is discussed in Sec. 5.5.

The background fit of the opposite sign opposite flavour lepton pairs is shown in Fig. 2(b). We obtain a total number of background events of

$$n_{Bkg} = 234 \pm 15, \tag{11}$$

which is in agreement with the expected number from MC truth. The number of background events in the signal region from 0 to 80 GeV in m_{ll} yields a value of

$$n_{Bkg,0-80} = 144 \pm 12. \tag{12}$$

5.3 Significance

The significance at LM0 point has been calculated once including shape information and once from simple event counting. The significance is quoted for the signal decay only and not for a general SUSY excess over the Standard Model. The calculation of the signal significance including shape information (σ_{Shape}) uses signal and background probability density functions and the pseudo datapoints. Given the background only hypothesis (fitted from the opposite sign opposite flavour lepton distribution) the significance of the signal plus background hypothesis given the pseudo datapoints is calculated based on the likelihood ratio. We observe a nominal significance of

$$\sigma_{Shape} = 6.7 \tag{13}$$

This significance is compared to the calculation from the number of signal and background events only (σ_{Count}). The number of background events is determined by integration over the background model in the region between 0 and 80 GeV. The number of signal events is determined by the fit. Since the number of background events has been fitted from data the method Z_{Bi} described in [17] has been used to calculate the significance. Here we use a scaling factor $\tau = 1$ to predict the number of background events and calculate the excess of events over this background. Using the number of events only we observe a nominal significance of

$$\sigma_{Count} = 4.4 \tag{14}$$

5.4 Systematic uncertainty of the significance

The main source for systematic uncertainties is the jet energy scale uncertainty. It is assumed to be 5% at an integrated luminosity of 200 pb^{-1} [12]. Due to the way the missing transverse energy corrections are implemented it is anti-correlated with MET:

$$\vec{\not{E}}_T^{corr} = \vec{\not{E}}_T - \sum_{i=1}^{N_{jets}} [\vec{p}_{T_i}^{corr} - \vec{p}_{T_i}^{raw}]. \tag{15}$$

This correlation has been taken into account. All jets above the threshold of 30 GeV which do not overlap with an electron are shifted by $\pm 5\%$ in energy which propagates into the MET calculation.

Evaluating the uncertainty on the number of events due to the uncertainty of the jet energy scale one obtains the numbers shown in Tab. 5. The variation in the number of events leads to different observed significances in the experiment.

The minimal observed significance for 200 pb^{-1} is 5.6 σ from shape information and 4.4 σ from pure event counting.

Table 5: Systematic uncertainties on the jet energy scale and their impact on the number of events at LM0. The quoted significance is in terms of standard deviations.

JES	N_{Sig}	$N_{Bkg,0-80}$	N_{Bkg}	N_Z	σ_{Count}	σ_{Shape}
0.05	76 ± 12	107 ± 10	170 ± 13	0 ± 7	4.4	5.6
$\pm$0.00	85 ± 13	144 ± 12	234 ± 15	0 ± 4	4.3	6.6
-0.05	114 ± 14	169 ± 13	272 ± 15	5 ± 4	5.3	8.0

Another source for systematic uncertainty is the arbitrariness of the background model. To evaluate the impact of the background model on the significance a different background model is tested. We use a Landau function to fit the flavour symmetric background and compare the outcome of the fit. We observe a significance of 5.3σ in case of a fit with a Landau function.

To evaluate the impact of theoretical uncertainties on the cross-section of the background processes each sample has been scaled by $\pm 10\%$. The impact of this variation is found to be negligible since the dominant background is SUSY itself at LM0. Other sources for systematic uncertainties (e.g. luminosity) have not been taken into account because the background is measured directly from data.

5.5 Systematic uncertainty on the endpoint

To evaluate the systematic uncertainty on the dilepton invariant mass endpoint the same uncertainty on the jet energy scale as in Sec. 5.4 is assumed. Additionally an electron energy scale uncertainty of 0.3% is assumed.

To evaluate the uncertainty due to the fit model itself the impact of the resolution model has been studied by varying the obtained fit values within their errors. The impact of the uncertainty in the efficiency measurement has been tested. For both electrons and muons the efficiency is scaled by $\pm 5\%$. The impact of these variations on the dilepton endpoint is displayed in Tab. 6.

Table 6: Systematic uncertainties on the determination of the dilepton endpoint $m_{ll,max}$.

Variation	Nominal	+ Var.	-Var.
Jet energy scale	48.0 ± 1.4	48.7 ± 1.4	49.5 ± 1.3
Electron energy scale	48.0 ± 1.4	47.9 ± 1.4	48.1 ± 1.4
Resolution model	48.0 ± 1.4	47.5 ± 0.4	-
Muon Efficiency	48.0 ± 1.4	48.1 ± 1.4	47.9 ± 1.4
Electron Efficiency	48.0 ± 1.4	48.1 ± 1.4	47.9 ± 1.4
Background model	48.0 ± 1.4	47.6 ± 1.8	-
Lepton acceptance	48.0 ± 1.4	49.3 ± 1.7	-

The main impact results from the bias which is introduced by the fit itself. To evaluate the bias we split the full LM0 dataset into 6 pieces of 200 pb^{-1} each. In each of the subsamples the fit is repeated. The outcome of the fits is shown in Tab. 7. All fits are statistically compatible but biased to lower values of m_{ll} compared to the theoretical value of the endpoint.

Table 7: Systematic bias on the determination of the dilepton endpoint $m_{ll,max}$.

Fit No.	0	1	2	3	4	5
$m_{ll,max}$ [GeV]	48.0 ± 1.4	47.9 ± 1.1	46.6 ± 0.7	51.0 ± 1.0	47.0 ± 0.9	48.6 ± 1.3

We use the mean (48.2 GeV) of the fits as an estimator of the systematic bias on the fitted endpoint which is found to be 4.5 GeV (compared to the theoretical value). The bias is included as an extra systematic uncertainty in Sec. 5.4.

This error can be reduced when more data is available or other input values are used. With more data one can distinguish between the different decay modes using the information of the whole invariant mass distribution and not only the endpoint.

5.6 Higher integrated luminosity

At the benchmark points LM1 and LM9 a higher integrated luminosity is necessary to measure the endpoint. Nevertheless the points can be discovered allready at an integrated luminosity of

500 pb^{-1}. For the evaluation of the significance the same method as for LM0 is used (Sec. 5.4). The observed significances at LM1 and LM9 for 500 pb^{-1} are listed in Tab. 8.

Table 8: Significance of the signal at LM1 and LM9 for 500 pb^{-1} for both methods. Both the minimal observed significance and the nominal significance are quoted.

	Nom. σ_{Shape}	Nom. σ_{Count}	Min. σ_{Shape}	Min. σ_{Count}
LM1	6.3	6.1	4.7	5.6
LM9	7.8	4.8	6.8	4.5

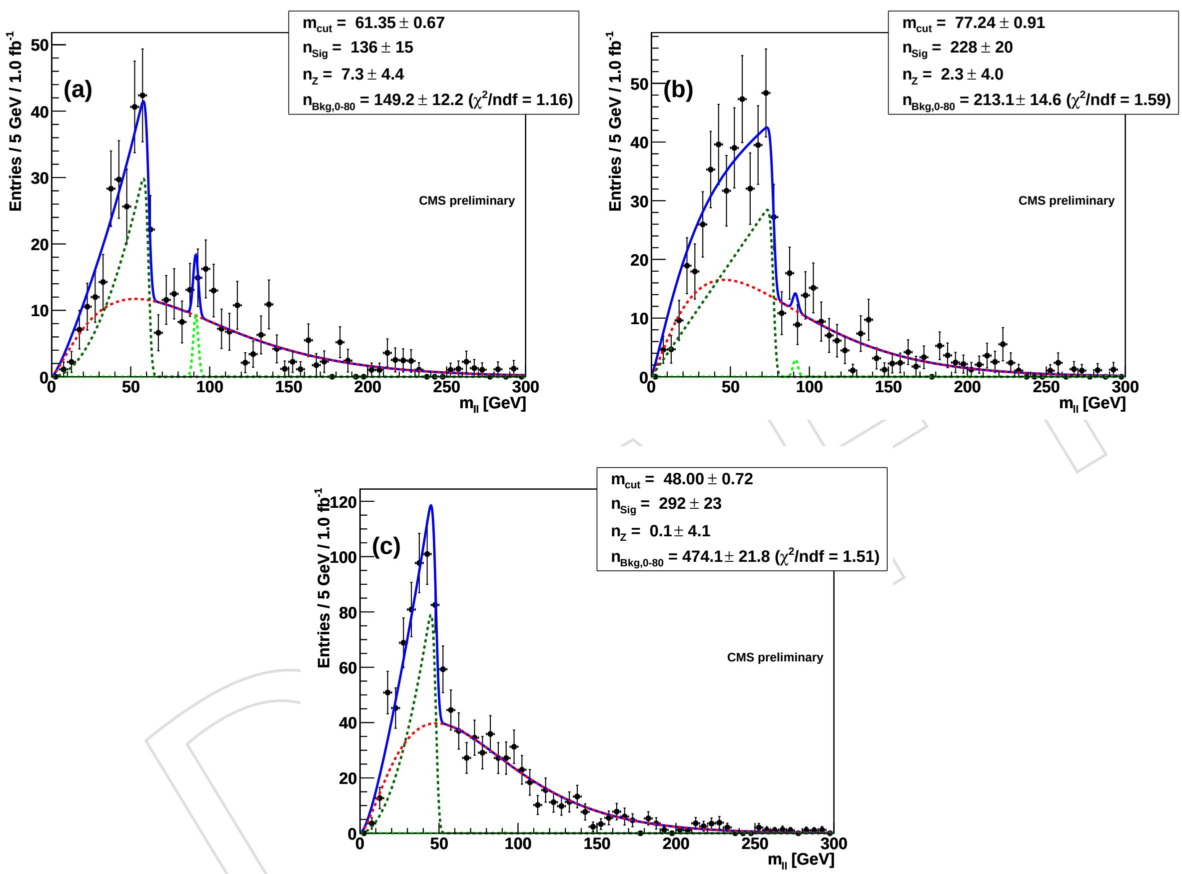

Figure 3: Final fits to the opposite sign same flavour invariant mass distribution at LM9 (a) where the signal model consists of a quadratic term, at LM1 (b) where the signal model is a triangle and at LM0 (c), for 1 fb^{-1}.

The fit of the invariant mass distribution at LM9 using an integrated luminosity of 1 fb^{-1} is shown in Fig. 3(a). It yields a value of

$$m_{ll,max} = \left(61.4 \pm 0.7_{stat.} \pm 0.9_{syst.}\right)\ \text{GeV}. \tag{16}$$

The theory value of $m_{ll,max} = 62,7$ GeV is reproduced within the error.

At LM1 a triangle is used as signal model and the fit of the invariant mass distribution at LM1 is shown in Fig. 3(b). It yields a value of

$$m_{ll,max} = \left(77.2 \pm 0.9_{stat.} \pm 1.0_{syst.}\right)\ \text{GeV}. \tag{17}$$

The theoretical endpoint of $m_{ll,max} = 78.2$ GeV is reproduced within the statistical error. The systematical error in both cases is evaluated as for LM0 in Sec. 5.5.

At LM0 the fit to the invariant mass distribution using an integrated luminosity of 1 fb^{-1} is shown in Fig. 3(c). It yields a value of

$$m_{ll,max} = \left(48.0 \pm 0.7_{stat.} \pm 1.2_{syst.}\right)\ \text{GeV}. \tag{18}$$

One can see that the bias towards lower values in the endpoint is still visible.

6 Conclusion

A significant excess of SUSY opposite sign same flavour lepton pairs can be found within the first 200 pb^{-1} at LM0. The signal provides a quite robust signature and the background determination directly from data is possible. The nominal observed significance of the signal using shape information is 6.7 σ and the minimal observed significance is 5.3 σ. The significance using only the number of observed events yields a minimal value of 4.4σ.

At the other studied benchmark points we observe a nominal significance using shape information of 6.3 σ (LM1) and 7.8 σ (LM9) for 500 pb^{-1}. The signifcance using only the number of observed events yields a value of 6.1 σ for LM1 and 4.8 σ for LM9, respectively.

We presented an unbinned maximum likelihood fit to the dilepton invariant mass distribution (corrected for the diefference in muon and electron reconstruction efficiency) with a data-driven resolution determination. At LM0 the combined fit of the diletonic endpoint is possible with 200 pb^{-1}. We obtain a value of

$$m_{ll,max} = \left(48.0 \pm 1.4_{stat.} \pm 2.2_{syst.} \pm 4.5_{bias.}\right)\ \text{GeV}, \tag{19}$$

compared to a theoretical value of 52.7 GeV. The main systematic bias arises from the fit model itself, which leads to a bias towards lower values since at LM0 the sharp endpoint is not present.

At the benchmark points LM9 and LM1 the endpoint can be measured with an integrated luminosity of 1 fb^{-1}.

References

[1] B. C. Alanach, "SOFTSUSY: a program for calculating supersymmetric spectra," *Comput.Phys.Commun.* **143** (2002) 305–331.

[2] A. Djouadi et al., "Decays of Supersymmetric Particles: the program SUSY-HIT (SUspect-SdecaY-Hdecay-InTerface)," *ActaPhys.Polon.B* **38** (2007) 635–644.

[3] T. Sjostrand et al., "PYTHIA 6.4 Physics and Manual," *JHEP* **0605:026** (2006).

[4] W. Beenakker et al., "Squark and Gluino Production at Hadron Colliders," *Nucl.Phys.B* **492** (1997) 51–103.

[5] **CMS** Collaboration, "Study of the Z production in association with jets in proton-proton collisions at $\sqrt{s} = 10$ TeV with the CMS detector at the CERN LHC," *CMS Physics Analysis Summary* **JME-08-006** (2008).

[6] J. Alwall et al., "MadGraph/MadEvent v4: The New Web Generation," *JHEP* **0709:028** (2007).

[7] M. Cacciari et al., "Updated predictions for the total production cross sections of top and of heavier quark pairs at the Tevatron and at the LHC," *JHEP* **0809:127** (2008).

[8] S. Frixione and M. L. Mangano, "How accurately can we measure the W cross section?," *JHEP* **0405:056** (2004).

[9] E. James et al., "Muon Identification in CMS," *CMS Note* **2006/010** (2006).

[10] S. Baffioni et al., "Electron Reconstruction in CMS," *CMS Note* **2006/040** (2006).

[11] G. P. Salam and G. Soyez, "A practical Seedless Infrared-Safe Cone jet algorithm," *JHEP* **0705:086** (2007).

[12] **CMS** Collaboration, "Plans for Jet Energy Corrections at CMS," *CMS Physics Analysis Summary* **JME-07-002** (2007).

[13] **CMS** Collaboration, "$\not\!\!E_T$ performance in CMS," *CMS Physics Analysis Summary* **JME-07-001** (2007).

[14] **CMS** Collaboration, "Measuring Electron Efficiencies at CMS with Early Data," *CMS Physics Analysis Summary* **EGM-07-001** (2007).

[15] **CMS** Collaboration, "Dilepton + Jets + MET channel : Observation and Measurement of $\tilde{\chi}_2^0 \to \tilde{\chi}_1^0 ll$," *CMS Physics Analysis Summary* **SUS-08-001** (2008).

[16] W. Verkerke and D. Kirkby, "The RooFit toolkit for data modeling," *arXiv:physics/0306116* (2003).

[17] R. D. Cousins et al., "Evaluation of three methods for calculating statistical significance when incorporating a systematic uncertainty into a test of the background-only hypothesis for a Poisson process," *Nucl.Inst.A* **595** (2008) 480–501.

A Signal decay

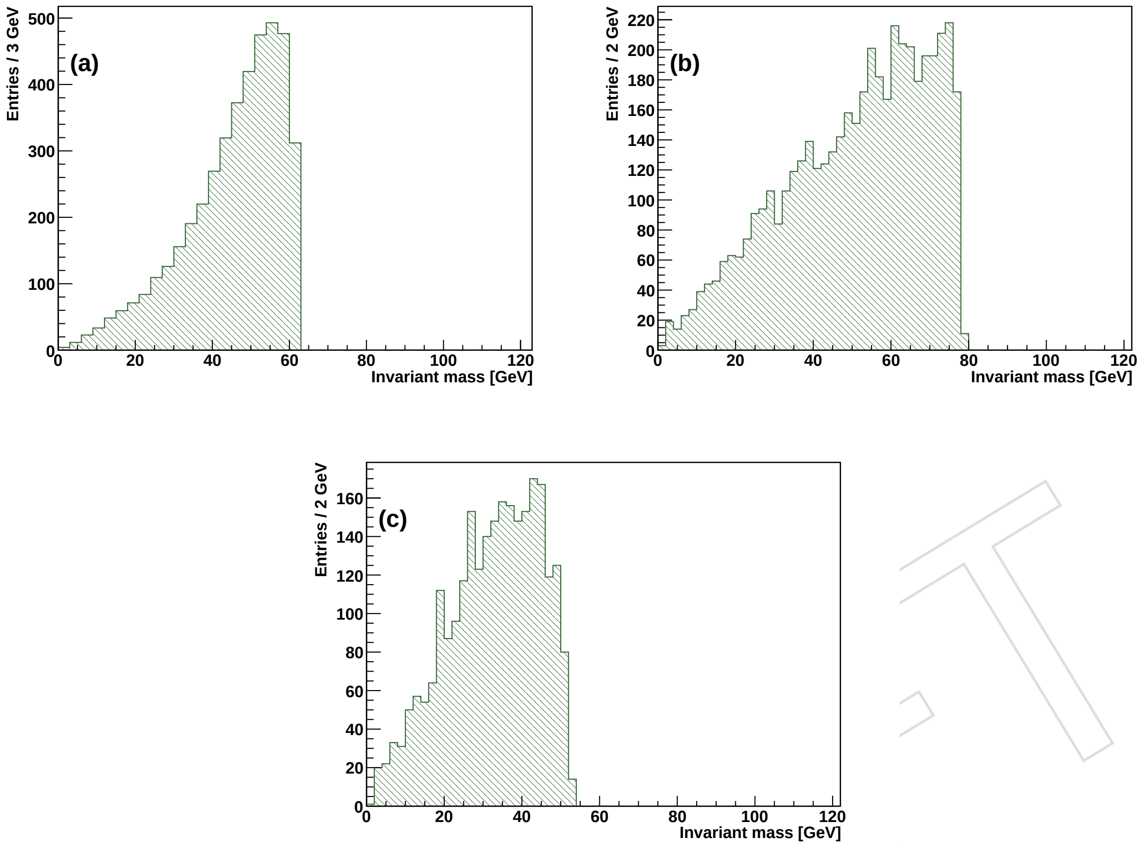

Figure 4: The invariant mass distribution of lepton pairs originating from signal decays in case of the 3-body decay at LM9 is shown in (a). The triangular shaped invariant mass distribution of lepton pairs in case of a 2-body decay at LM1 is shown in (b). The invariant mass distribution at LM0 (3-body decay) is shown in (c).

B Lepton isolation

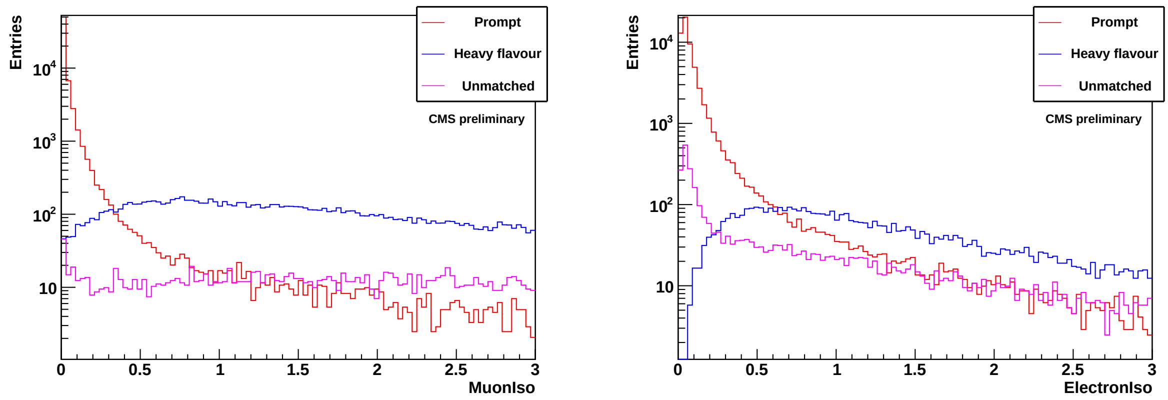

(a) (b)

Figure 5: Isolation value for muons (a) and electrons (b) passing the acceptance and identification cuts in $t\bar{t}$ and SUSY LM0 events. The red curve shows all leptons which can be matched onto a prompt lepton. The blue curve represents leptons matched onto leptons from decays of heavy resonances. Magenta are unmatched leptons, e.g. fake leptons from jets.

C Efficiency measurement

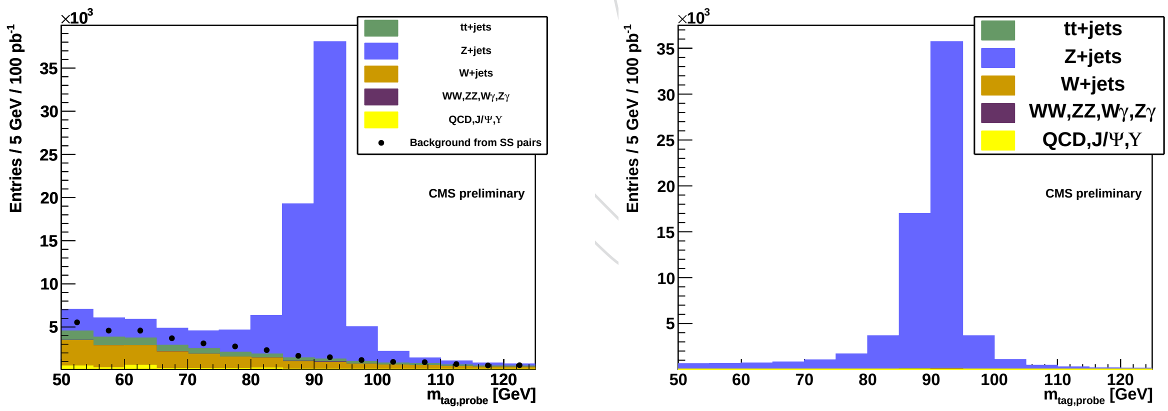

(a) (b)

Figure 6: The invariant mass of all muon tag and probe pairs is shown in (a). The black points represent the background estimation from the same sign tag and probe pairs. All pairs where the probe could be matched onto a reconstructed muon are shown in (b).

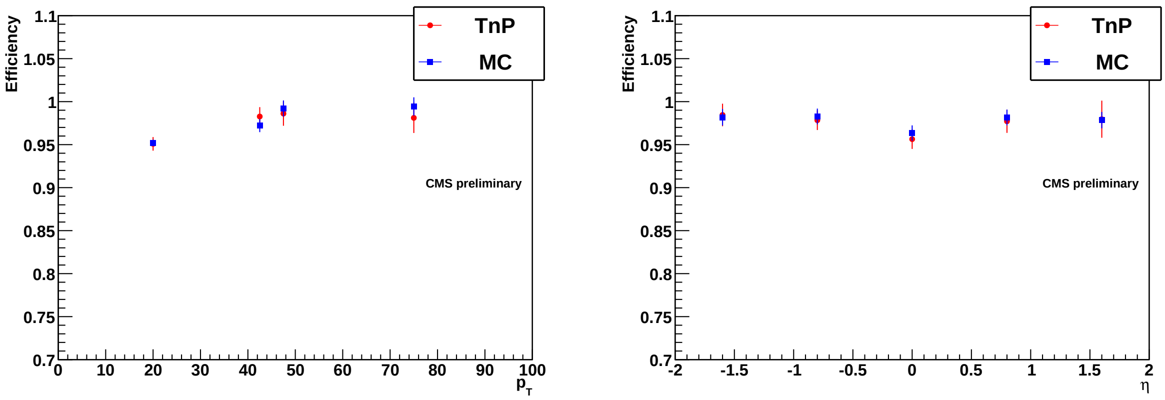

(a) (b)

Figure 7: Efficiency measurement by the tag and probe method for muons in comparison to MC truth, versus p_T (a) and η (b).

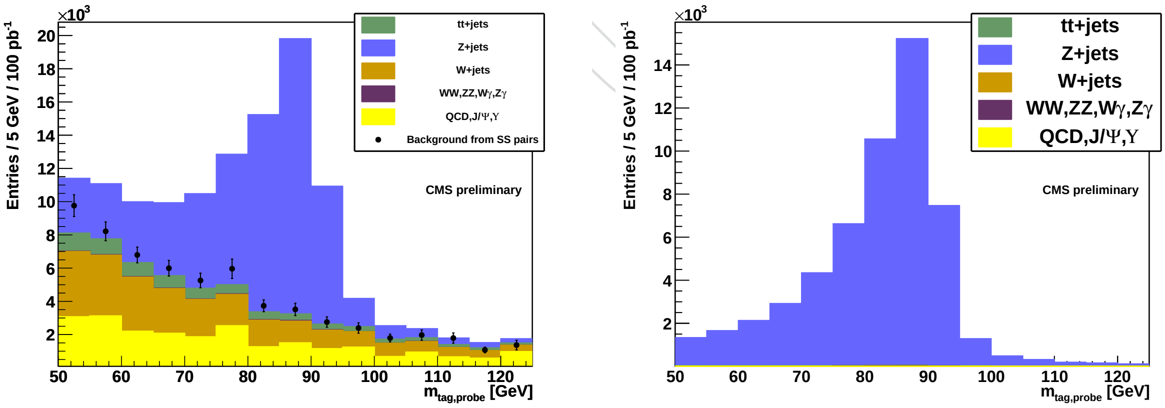

(a) (b)

Figure 8: The invariant mass of all electron tag and probe pairs is shown in (a). The black points represent the background estimation from the same sign tag and probe pairs. All pairs where the probe could be matched onto a reconstructed electron are shown in (b).

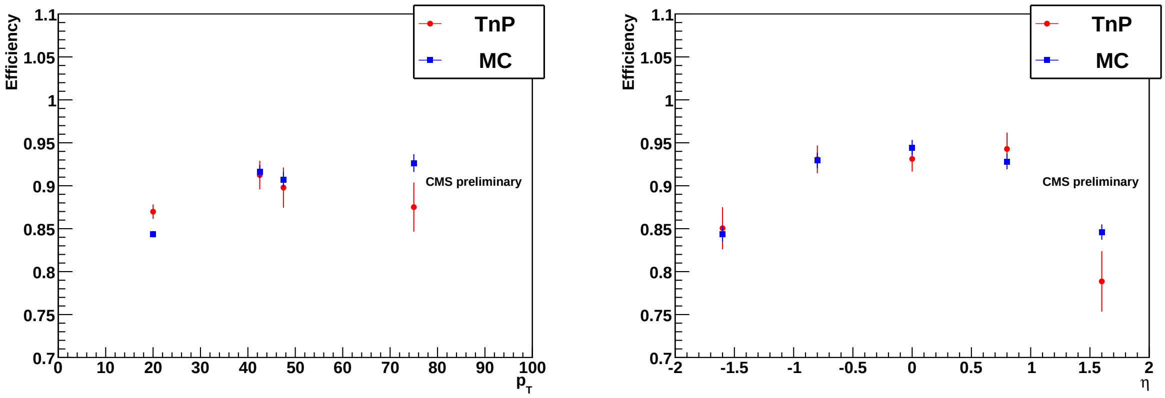

(a) (b)

Figure 9: Efficiency measurement by the tag and probe method for electrons in comparison to MC truth, versus p_T (a) and η (b).

D Resolution measurement

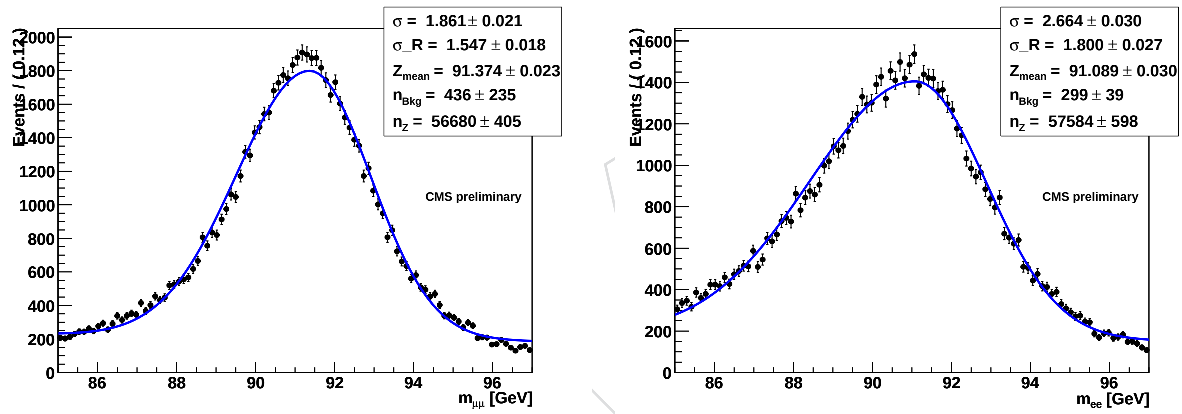

(a) (b)

Figure 10: Resolution measurement from Z events for muons (a) and electrons (b).